GSA DATA REPOSITORY 2020058 https://doi.org/10.1130/G46835.1

Supplementary information for: Oceanic slab-top melting during subduction: implications for trace-element recycling and adakite petrogenesis

David Hernández-Uribe[1*], Juan David Hernández-Montenegro[2], Kim A. Cone[1], and Richard M. Palin[1]

[1]*Department of Geology and Geological Engineering, Colorado School of Mines, 1500 Illinois St, Golden, CO 80401, USA*
[2]*Departamento de Geociencias, Universidad Nacional de Colombia, Bogotá, Colombia*

*Corresponding author: *dav.hernandez.uribe@gmail.com*

METHODS

Modeled bulk-rock compositions

Phase equilibrium modeling employed bulk compositions for the average N-MORB of Gale et al. (2013) and the 'supercomposite' basalt from Staudigel et al. (1989), which are given in Table DR1. These. The average N-MORB composition corresponds with the log-normal mean of mid-ocean ridge segments situated >500 km away from mantle plumes, and so is considered representative of the uppermost pristine basaltic part of the oceanic crust. On the other hand, the Staudigel et al. (1989) 'supercomposite' basalt is a proportional mix of various lithologies reported from ocean-floor drill cores, representing an average of the altered uppermost part composition of the oceanic crust. It is considered here as being the most representative example of hydrothermally altered basaltic oceanic crust reported in the literature.

The bulk-rock X_{Fe}^{3+} [$X_{Fe}^{3+} = Fe^{3+}/(Fe^{2+}+Fe^{3+})$] ratios for the average N-MORB was set to 0.16 based on a μ-XANES spectroscopy-derived global average constrained by Cottrell and Kelly (2011), whereas the modeled X_{Fe}^{3+} for the supercomposite was calculated from the bulk-rock $FeO:Fe_2O_3$ ratio reported from Staudigel et al. (1989). Water was considered in excess in all calculations up to the point of initial melting, when the H_2O content was fixed to allow minimal saturation at the pressure–temperature (*P–T*) conditions where the modeled geotherm crosses the wet solidus. While basaltic rocks are mostly anhydrous, MORB crystalizes in subaqueous environments, being subject to hydrothermal alteration (Alt et al., 1998), and as such, they might contain higher fluid contents at the onset of subduction than fresh and unaltered parent magmas that have been derived directly from the mantle; thus, we consider that the modeled MORB compositions are water saturated throughout our modeling.

Phase equilibrium modeling

All phase diagrams were constructed using Theriak-Domino (de Capitani and Brown, 1987; de Capitani and Petrakakis, 2010) and the internally consistent thermodynamic data set ds62 (Holland and Powell, 2011) in the 10-component Na_2O–CaO–K_2O–FeO–MgO–Al_2O_3–SiO_2–H_2O–TiO_2–O_2 (NCKFMASHTO) system. The following activity–composition (*a–x*) relations for solid-solution phases were used: clinopyroxene (diopside–omphacite–jadeite), clinoamphibole (glaucophane–actinolite–hornblende), and tonalitic melt (Green et al., 2016); garnet, biotite, muscovite–paragonite, and chlorite (White et al., 2014); epidote (Holland and Powell, 2011); plagioclase (Holland and Powell, 2003); ilmenite (White et al., 2000). Pure phases comprised chloritoid, talc, lawsonite, kyanite, quartz, rutile, titanite, and albite. Individual phase diagrams for each bulk composition are shown in Figure DR4.

Uncertainties related to the absolute positions of assemblage field boundaries on calculated phase diagrams have been shown to be less than ±1 kbar and ±50 °C at the 2σ level (Powell and Holland, 2008; Palin et al., 2016), with this variation being largely a function of propagated uncertainty on end-member thermodynamic properties within the data set. However, as all phase diagrams were calculated using the same dataset and *a–x* relations, similar absolute errors associated with dataset end-members cancel, and calculated phase equilibria are relatively accurate to within ±0.2 kbar and ±10–15 °C (Powell and Holland, 2008).

Trace-element modeling

Calculated compositions of melt formed along a hot geotherm for fresh and altered MORB are shown in the Figs 2 and DR3, and given in Table DR2. Modeling of trace elements was performed using the equation for modal melting of Shaw (2006) using mineral–melt partition coefficients from Bédard (2006). The subsolidus trace-element compositions of N-MORB and 'supercomposite' basalt were taken from Gale et al. (2013) and Staudigel et al. (1996), respectively. Melt extraction was not considered in our modeling, as calculated volumes along the considered geotherms did not reach the rheological melt-loss threshold for metamafic rocks of ~20 vol.% (Rushmer, 1995; Vigneresse et al., 1996), although in nature larger volumes may form and ultimately migrate away from the source.

Accessory phases, such as allanite, apatite, and zircon were not considered in trace-element modeling as current generations of *a–x* relations cannot constrain their stability—alongside other rare earth elements (REE)-bearing accessory phases—during subduction-zone metamorphism. Yet, we acknowledge that the stability of these mineral at suprasolidus conditions exerts a first-order control on the concentrations of trace elements in the melt. Apatite carries non-trivial amounts of large-ion lithophile elements (LILE) and REE, however, garnet may incorporate notable phosphorus at high *P–T* conditions, thereby reducing the stability of apatite at high pressure conditions (Konzett and Frost, 2009). Zircon hosts considerable amounts Zr and Hf (Bea *et al.,* 2006), whereas allanite is the main carrier of Th and light-REE in subducted metabasic rocks (Hermann, 2002). Thus, if these minerals are stable at suprasolidus

conditions, modeled melt compositions would be slightly more depleted in Zr, Hf, Th and light-REE than calculated (Fig. DR3).

CALCULATED MELT COMPOSITIONS

Partial melt compositions generated from both MORB types during hot subduction are shown in Figure DR3 and given in Table DR2. The initial melt calculated for pristine MORB is SiO_2- and alkali (Na_2O+K_2O)-rich (~72 wt%, and ~8wt%, respectively), and MgO- and FeO-poor (~0.04 wt% and ~1 wt%, respectively) (Fig. DR3 and Table DR2). As *P–T* increases, the SiO_2 content decreases down to ~69 wt%, whereas the MgO- and FeO-content increases up to 0.6 wt% and 2 wt%, respectively, until the end of the modeled *P–T* path (Fig. DR3 and Table DR2). The melt's alkali content decreases by ~1 wt% at ~31 kbar and 930 °C, after these *P–T* conditions, the alkali content sharply increase up to ~9 wt% (Fig. DR3 and Table DR2).

The initial melt calculated for the altered MORB is SiO_2- and alkali-rich (~71 wt%, and ~8wt%, respectively), and MgO- and FeO-poor (~0.02 wt% and ~0.04 wt%, respectively) (Fig. DR3 and Table DR2). As *P–T* increases, the SiO_2 content decreases down to ~68 wt%, whereas the MgO- and FeO content remain relatively constant, until the end of the modeled *P–T* path (Fig. DR3 and Table DR2). The melt's alkali content decreases by ~1 wt% at ~30 kbar and 920 °C, after these *P–T* conditions, the alkali content sharply increase up to ~9 wt% (Fig. DR3 and Table DR2).

In terms of the trace elements, the initial melts generated in both modeled compositions are characterized by relatively lower concentrations of Cs, Rb, Ba, Th, U, K, Nb, Ta, and LREE, and higher concentrations of HREE (Fig. DR3 and Table DR2). As *P–T* increases, the melts become relatively depleted in Cs, Rb, Ba, Th, U, K, Nb, Ta, and light REE, and enriched in heavy REE compared to the initial melts (Fig. DR3 and Table DR2).

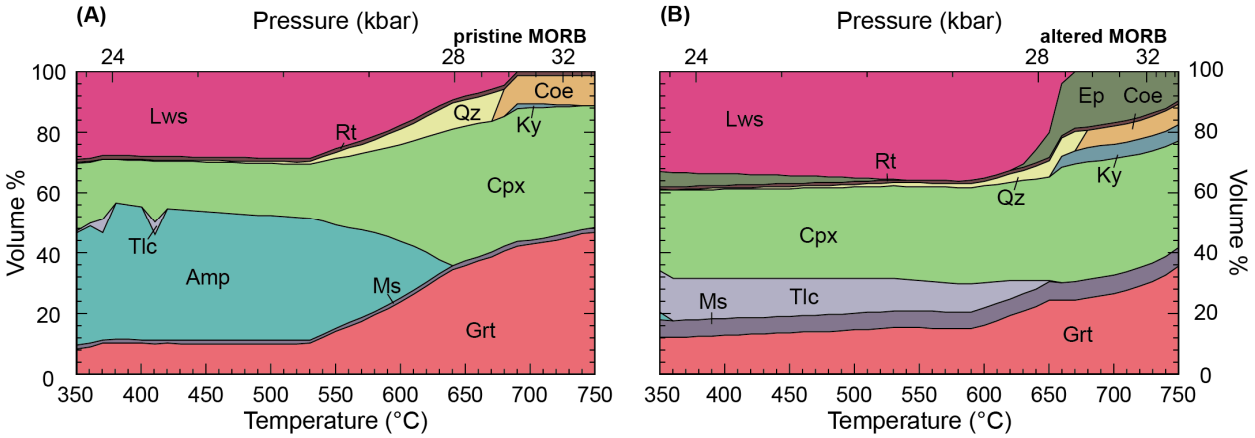

Figure DR1. Calculated phase assemblage changes along an average geotherm for (A) pristine MORB and (B) altered MORB. Mineral abbreviations follow Whitney and Evans (2010).

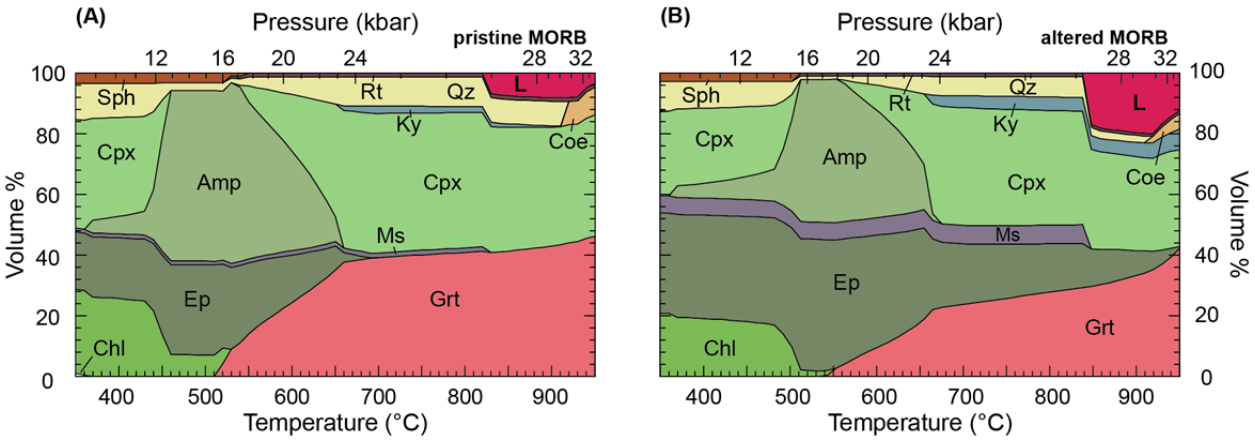

Figure DR2. Calculated phase assemblage changes along a hot geotherm for (A) pristine MORB and (B) altered MORB. Mineral abbreviations follow Whitney and Evans (2010), with the exception of "L" which refers to melt.

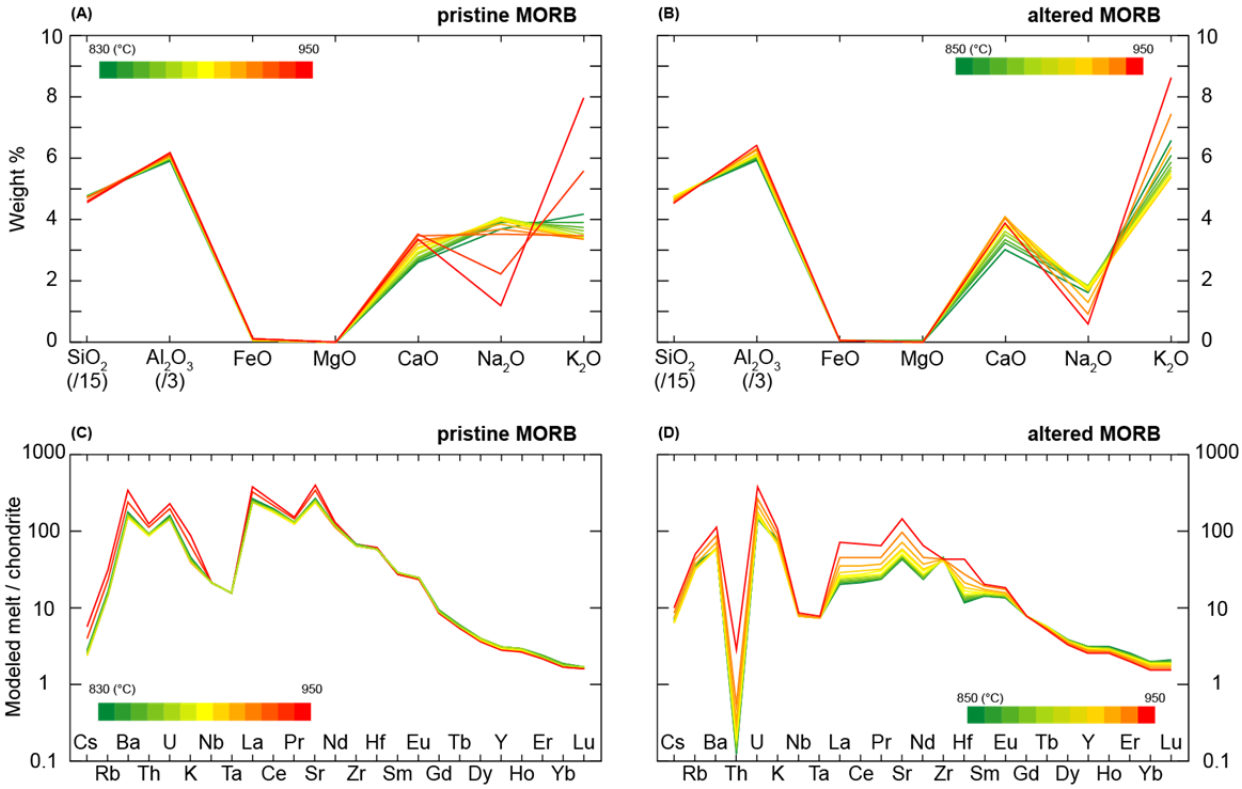

Figure DR3. Modeled major and trace-element compositions for (A and C) pristine MORB and (B and D) altered MORB. Trace-element patterns are chondrite normalized (McDonough and Sun, 1995).

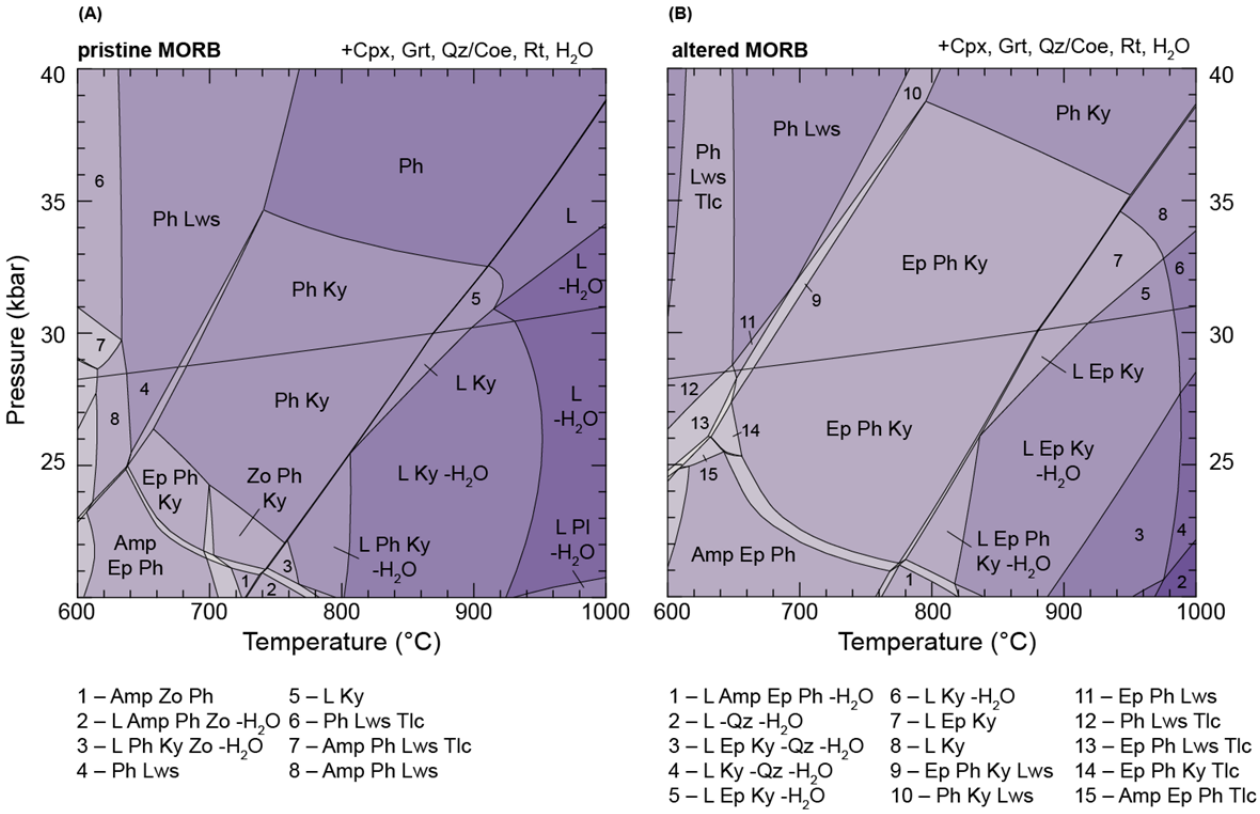

Figure DR4. Pressure–temperature phase equilibrium diagrams for (A) pristine MORB and (B) altered MORB. Mineral abbreviations follow Whitney and Evans (2010), with the exception of "L" which refers to melt.

Table DR1. Bulk-rock compositions used for phase equilibrium modeling (normalized mol%).

Sample	H_2O	SiO_2	Al_2O_3	CaO	MgO	FeO^{tot}	K_2O	Na_2O	TiO_2	O	X_{Fe}^{3+}	X_{Mg}	Note
	mol%												
G-13	14.00	45.21	7.99	10.91	10.37	7.36	0.08	2.46	1.03	0.59	0.16	0.59	subsolidus
S-89	13.92	43.05	8.60	12.97	9.33	7.09	0.34	1.89	0.83	1.98	0.56	0.57	subsolidus
G-13	3.04	50.98	9.01	12.29	11.69	8.29	0.09	2.77	1.16	0.66	0.16	0.59	suprasolidus[1]
S-89	8.09	45.97	9.18	13.85	9.96	7.57	0.36	2.01	0.89	2.11	0.56	0.57	suprasolidus[1]

FeO^{tot} is total iron expressed as FeO. Oxygen = O, which combines with FeO via the equation $2FeO + O = Fe_2O_3$; thus, bulk O is identically equal to bulk Fe_2O_3, while true bulk FeO is given by FeO^{tot}–2 X O. X_{Mg} = MgO/(MgO + FeO^{tot}), and X_{Fe}^{3+} ratios = (2 X O)/FeO^{tot}

[1]Minimum water to saturate at the solidus.

Table DR1. Bulk-rock compositions used for phase equilibrium modelling (normalized wt%). G-13 = pristine MORB (Gale et al., 2013); S-89 = altered MORB (Staudigel et al., 1989).

Table DR2. Modeled major (normalized wt% on an anhydrous basis) and trace-element compositions (ppm) of modeled melts along the hot geotherm.

Pristine														**Altered**										
P–T (kbar, °C)	26.8, 830	26.9, 840	27.1, 850	27.3, 860	27.6, 870	27.9, 880	28.4, 890	28.9, 900	29.6, 910	30.4, 920	31.4, 930	32.6, 940	34, 950	27.1, 850	27.3, 860	27.6, 870	27.9, 880	28.4, 890	28.9, 900	29.6, 910	30.4, 920	31.4, 930	32.6, 940	34, 950
wt %																								
SiO_2	71.56	71.52	71.43	71.35	71.28	71.23	71.18	71.16	71.16	71.15	70.87	69.74	68.58	70.92	70.99	70.91	70.83	70.75	70.67	70.61	70.53	69.63	68.68	67.74
Al_2O_3	17.77	17.86	17.94	18.01	18.08	18.13	18.17	18.20	18.21	18.23	18.38	18.58	18.63	17.78	17.89	18.00	18.09	18.18	18.25	18.31	18.37	18.65	18.90	19.12
FeO	0.09	0.09	0.10	0.10	0.11	0.12	0.12	0.13	0.14	0.15	0.17	0.17	0.18	0.04	0.04	0.04	0.04	0.04	0.04	0.04	0.04	0.04	0.04	0.03
MgO	0.04	0.04	0.04	0.04	0.04	0.04	0.05	0.05	0.05	0.05	0.06	0.06	0.06	0.02	0.02	0.02	0.02	0.02	0.02	0.02	0.02	0.02	0.02	0.02
CaO	2.62	2.68	2.75	2.81	2.88	2.96	3.04	3.13	3.23	3.34	3.47	3.56	3.39	3.03	3.20	3.34	3.48	3.61	3.75	3.89	4.03	4.06	4.02	3.89
Na_2O	3.73	3.91	3.98	4.03	4.06	4.06	4.03	3.96	3.85	3.70	3.55	2.28	1.22	1.63	1.79	1.82	1.83	1.82	1.78	1.73	1.65	1.27	0.90	0.59
K_2O	4.20	3.90	3.76	3.64	3.54	3.46	3.40	3.37	3.36	3.39	3.51	5.61	7.95	6.57	6.06	5.88	5.72	5.58	5.48	5.40	5.36	6.33	7.45	8.61
ppm																								
Cs	0.53	0.52	0.51	0.49	0.48	0.47	0.47	0.46	0.46	0.47	0.48	0.76	1.07	1.37	1.27	1.24	1.21	1.19	1.17	1.15	1.15	1.35	1.59	1.85
Rb	38	37	36	36	35	34	34	34	34	34	35	53	72	84	78	76	74	73	72	71	70	83	97	112
Ba	423	413	402	392	384	377	372	370	369	372	382	595	823	138	133	133	133	134	135	138	141	169	207	263
Th	2.73	2.70	2.67	2.64	2.62	2.60	2.59	2.59	2.59	2.61	2.65	3.27	3.70	0.003	0.004	0.004	0.004	0.005	0.005	0.006	0.007	0.009	0.015	0.078
U	1.17	1.16	1.14	1.12	1.10	1.09	1.08	1.07	1.07	1.08	1.10	1.44	1.71	1.02	1.01	1.03	1.06	1.10	1.14	1.20	1.27	1.52	1.91	2.68
K	25308	24702	24038	23445	22938	22530	22235	22068	22042	22184	22810	35657	49487	42939	39790	38799	37918	37165	36555	36101	35840	42218	49681	57535
Nb	5.05	5.04	5.03	5.02	5.01	5.00	5.00	4.99	4.99	4.99	5.00	5.11	5.17	1.80	1.78	1.78	1.78	1.77	1.77	1.77	1.78	1.83	1.88	1.93
Ta	0.21	0.21	0.21	0.21	0.21	0.21	0.21	0.21	0.21	0.21	0.21	0.21	0.22	0.10	0.10	0.10	0.10	0.10	0.10	0.10	0.10	0.10	0.10	0.10
La	62	61	60	59	58	57	56	56	56	56	57	76	91	4.72	4.76	4.91	5.10	5.33	5.63	6.01	6.52	7.92	10.36	16.15
Ce	119	118	116	115	114	113	112	111	111	111	113	134	148	13	13	13	14	15	15	16	18	21	27	40
Pr	12	12	12	12	12	12	12	12	12	12	12	13	14	2.07	2.10	2.17	2.25	2.35	2.48	2.64	2.85	3.34	4.13	5.77
Sr	1943	1911	1875	1843	1815	1792	1776	1766	1765	1774	1809	2432	2934	301	304	313	325	340	358	383	415	505	661	1034
Nd	56	55	55	54	54	54	53	53	53	53	53	58	60	10	10	11	11	12	12	13	14	16	20	28
Zr	258	256	255	253	252	250	249	248	246	245	245	254	258	170	165	162	160	158	156	154	152	156	159	160
Hf	6.15	6.12	6.09	6.06	6.03	6.01	5.98	5.96	5.94	5.93	5.94	6.15	6.26	1.16	1.19	1.25	1.31	1.39	1.49	1.62	1.80	2.12	2.70	4.18
Sm	4.35	4.32	4.29	4.27	4.24	4.22	4.19	4.17	4.14	4.11	4.10	4.14	4.15	2.05	2.06	2.09	2.13	2.17	2.23	2.29	2.37	2.51	2.69	2.94
Eu	1.43	1.42	1.41	1.40	1.40	1.39	1.38	1.37	1.36	1.36	1.35	1.36	1.36	0.74	0.74	0.75	0.76	0.78	0.79	0.81	0.83	0.87	0.92	0.99
Gd	1.88	1.87	1.86	1.85	1.84	1.83	1.81	1.80	1.79	1.77	1.77	1.75	1.74	1.47	1.46	1.46	1.46	1.46	1.46	1.46	1.46	1.47	1.47	1.47
Tb	0.22	0.21	0.21	0.21	0.21	0.21	0.21	0.21	0.20	0.20	0.20	0.20	0.20	0.20	0.20	0.20	0.20	0.20	0.20	0.19	0.19	0.19	0.19	0.18
Dy	1.00	0.99	0.99	0.98	0.97	0.97	0.96	0.95	0.95	0.94	0.93	0.92	0.92	0.92	0.91	0.90	0.89	0.88	0.87	0.86	0.84	0.83	0.81	0.78
Y	4.96	4.92	4.89	4.86	4.83	4.80	4.77	4.73	4.69	4.65	4.63	4.57	4.54	4.77	4.70	4.64	4.58	4.51	4.45	4.38	4.31	4.22	4.10	3.94
Ho	0.16	0.16	0.16	0.16	0.16	0.16	0.16	0.16	0.15	0.15	0.15	0.15	0.15	0.16	0.16	0.16	0.16	0.15	0.15	0.15	0.15	0.14	0.14	0.13
Er	0.39	0.38	0.38	0.38	0.38	0.37	0.37	0.37	0.37	0.36	0.36	0.36	0.35	0.39	0.38	0.37	0.37	0.36	0.36	0.35	0.34	0.33	0.32	0.31
Yb	0.30	0.30	0.30	0.30	0.29	0.29	0.29	0.29	0.29	0.28	0.28	0.28	0.28	0.31	0.31	0.30	0.30	0.29	0.29	0.28	0.27	0.27	0.26	0.24
Lu	0.04	0.04	0.04	0.04	0.04	0.04	0.04	0.04	0.04	0.04	0.04	0.04	0.04	0.05	0.05	0.05	0.05	0.04	0.04	0.04	0.04	0.04	0.04	0.04
X_{Mg}	0.29	0.29	0.29	0.28	0.28	0.28	0.27	0.27	0.27	0.26	0.26	0.25	0.24	0.36	0.36	0.36	0.36	0.35	0.35	0.35	0.34	0.34	0.33	0.33
La/Yb	204	202	200	197	196	194	194	194	196	198	203	274	329	15	15	16	17	18	20	21	24	30	40	66

1

2 **Table DR2.** Modeled major (normalized wt% on an anhydrous basis) and trace-element compositions (ppm) of modeled melts along
3 the hot geotherm.

REFERENCES

Alt, J. C., Teagle, D. A., Brewer, T., Shanks III, W. C., and Halliday, A., 1998, Alteration and mineralization of an oceanic forearc and the ophiolite-ocean crust analogy. Journal of Geophysical Research: Solid Earth 103(B6), 12365–12380.

Bédard, J.H., 2006, A catalytic delamination-driven model for coupled genesis of Archaean crust and sub-continental lithospheric mantle. Geochimica et Cosmochimica Acta 70, 1188–1214.

Bea, F., Montero, P., and Ortega, M., 2006, A LA–ICP–MS evaluation of Zr reservoirs in common crustal rocks: Implications for Zr and Hf geochemistry, and zircon-forming processes. The Canadian Mineralogist, 44(3), 693–714.

Cottrell, E., and Kelley, K. A., 2011, The oxidation state of Fe in MORB glasses and the oxygen fugacity of the upper mantle. Earth and Planetary Science Letters 305(3), 270–282.

de Capitani, C., and Brown, T. H., 1987, The computation of chemical equilibrium in complex systems containing non-ideal solutions. Geochimica et Cosmochimica Acta 51, 2639–2652.

de Capitani, C., and Petrakakis, K., 2010, The computation of equilibrium assemblage diagrams with Theriak/Domino software. American Mineralogist 95(7), 1006–1016.

Engi, M., 2017, Petrochronology based on REE-minerals: monazite, allanite, xenotime, apatite. Reviews in Mineralogy and Geochemistry 83(1), 365–418.

Gale, A., Dalton, C. A., Langmuir, C. H., Su, Y., and Schilling, J. G., 2013, The mean composition of ocean ridge basalts. Geochemistry, Geophysics, Geosystems 14(3), 489–518.

Green, E. C. R. et al., 2016, Activity–composition relations for the calculation of partial melting equilibria in metabasic rocks. Journal of Metamorphic Geology 34, 845–869.

Hermann, J., 2002, Allanite: thorium and light rare earth element carrier in subducted crust. Chemical Geology 192(3–4), 289–306.

Holland, T. J. B., and Powell, R., 2003, Activity–composition relations for phases in petrological calculations: an asymmetric multicomponent formulation. Contributions to Mineralogy and Petrology 145(4), 492–501.

Holland, T. J. B., and Powell, R., 2011, An improved and extended internally consistent thermodynamic dataset for phases of petrological interest, involving a new equation of state for solids. Journal of Metamorphic Geology 29, 333–383.

Konzett, J., and Frost, D. J., 2009, The High P–T Stability of Hydroxyl-apatite in Natural and Simplified MORB—an Experimental Study to 15 GPa with Implications for Transport and Storage of Phosphorus and Halogens in Subduction Zones. Journal of Petrology 50, 2043–2062.

McDonough, W. F., and Sun, S. S., 1995, The composition of the Earth. Chemical Geology 120(3–4), 223–253.

Palin, R. M., Weller, O. M., Waters, D. J., and Dyck, B., 2016, Quantifying geological uncertainty in metamorphic phase equilibria modelling; a Monte Carlo assessment and implications for tectonic interpretations. Geoscience Frontiers 7, 591–607.

Powell, R., and Holland, T. J. B., 2008, On thermobarometry. Journal of Metamorphic Geology 26, 155–179.

Rushmer, T., 1995, An experimental deformation study of partially molten amphibolite: Application to low-melt fraction segregation. Journal of Geophysical Research: Solid Earth, 100(B8), 15681–15695.

Shaw, D.M., 2006, Trace elements in magmas: a theoretical treatment. Cambridge University Press.

Spear, F. S., 2010, Monazite–allanite phase relations in metapelites. Chemical Geology, 279(1–2), 55–62.

Staudigel, H., Hart, S. R., Schmincke, H. U., and Smith, B. M., 1989, Cretaceous ocean crust at DSDP Sites 417 and 418: Carbon uptake from weathering versus loss by magmatic outgassing. Geochimica et Cosmochimica Acta 53(11), 3091–3094.

Staudigel, H., Plank, T., White, B., and Schmincke, H. U., 1996, Geochemical fluxes during seafloor alteration of the basaltic upper oceanic crust: DSDP Sites 417 and 418. Subduction: top to bottom 96, 19–38.

Vigneresse, J. L., Barbey, P., and Cuney, M., 1996, Rheological transitions during partial melting and crystallization with application to felsic magma segregation and transfer. Journal of Petrology, 37(6), 1579–1600.

White, R. W., et al., 2014, New mineral activity–composition relations for thermodynamic calculations in metapelitic systems. Journal of Metamorphic Geology 32, 261–286.

White, R. W., Powell, R., Holland, T. J. B. and Worley, B. A., 2000, The effect of TiO_2 and Fe_2O_3 on metapelitic assemblages at greenschist and amphibolite facies conditions: mineral equilibria calculations in the system K_2O–FeO–MgO–Al_2O_3–SiO_2–H_2O–TiO_2–Fe_2O_3. Journal of Metamorphic Geology 18, 497–511.

Whitney, D.L., and Evans, B.W., 2010, Abbreviations for names of rock–forming minerals. American Mineralogist 95, 185–187.